ARTICLE NO. 80-4102

C80-126

Stability and Control Characteristics of the Aerocrane Hybrid Heavy-Lift Vehicle

00017
00018
00020

H. C. Curtiss, Jr.* and W. F. Putman†
Princeton University, Princeton, N.J.

A series of experiments were conducted with a dynamically scaled free-flight model of a unique hybrid heavy-lift vehicle, the Aerocrane, to determine its stability and control characteristics. A theoretical model was developed to predict these characteristics which showed very good agreement with experiment. The results of a study of the precision hover capabilities of the Aerocrane, based on this theoretical model, are described. It is shown that the precision hover capabilities are similar to those predicted for helicopters which can lift a comparable payload.

Nomenclature

a = rotor blade lift curve slope
A_1, B_1 = rotor cyclic pitch
C_D = centerbody drag coefficient
C_H, C_Y = rotor in-plane force coefficients, $C_H, C_Y = (H, Y)/[\rho\pi R^2(\Omega R)^2]$
C_{L_M} = centerbody Magnus force coefficient
C_M, C_L = rotor hub moment coefficients, $C_M, C_L = (M_H, L_H)/[\rho\pi R^2(\Omega R)^2 R]$
C_T = rotor thrust coefficient, $C_T = T_s/\rho\pi R^2(\Omega R)^2$
f_n = $1-(R_B/R)^n$
F_B = centerbody buoyant force
I_0 = vehicle pitch/roll inertia
I_z = vehicle moment of inertia about axis of rotation
j = proportionality factor between harmonic induced velocity and aerodynamic moments
m_A = apparent mass of centerbody
m_0 = vehicle mass
p = vehicle roll rate, $p=\dot{\phi}$
q = vehicle pitch rate, $q=\dot{\theta}$
r_0 = displacement of center of gravity below center of buoyancy
R = rotor radius
R_B = centerbody radius
T_s = rotor thrust
u = vehicle translational velocity
v = vehicle lateral velocity
V = centerbody volume
W = vehicle weight
x = fractional rotor radius
θ = vehicle pitch attitude, positive nose up
θ_0 = rotor collective pitch
$\lambda_0, \lambda_B, \lambda_M, \lambda_L$ = steady and harmonic components of induced velocity
μ_s = rotor advance ratio
ρ = air density
σ = rotor solidity, $\sigma = bc/\pi R$
ϕ = vehicle roll attitude, positive roll right
ψ_w = blade azimuth angle measured from downwind in direction of rotation
Ω = rotor/centerbody angular velocity

Superscript

$(\bar{\ })$ = velocity nondimensionalized by ΩR

Subscript

s,w = referenced to a wind-body axis, i.e., $x_{s,w}$ axis points into the relative wind and the $z_{s,w}$ axis lies along the axis of rotation

Rotor blade pitch is given by the expression,

$$\theta = \theta_0 - A_{1_{s,w}}\cos\psi_w - B_{1_{s,w}}\sin\psi_w$$

Introduction

THE Aerocrane is a unique hybrid heavy-lift vehicle designed to lift and transport heavy loads through a combination of aerostatic and aerodynamic lift. It is also one of the few new hybrid heavy-lift concepts that has been the subject of extensive experimental and theoretical studies.[1-3] These studies were directed toward the development of an experimentally verified theoretical model of the flight mechanics of the concept, such that the essential element in the viability of any hybrid heavy-lift concept, its precision hover capabilities could be studied and evaluated.

The Aerocrane concept, in its simplest form, shown in Fig. 1, consists of a spherical, helium-filled centerbody with rotating wings mounted on the equator of the sphere. The entire lifting assembly rotates, propelled by engines mounted near the tips of the rotating wings. A nonrotating gondola or pilot's station is provided below the spherical centerbody. Vertical equilibrium and height control is obtained by collective pitch on the rotating wings and translational or maneuvering control is provided in one of two ways. Cyclic pitch variation on the rotating wings can be employed to provide moments on the vehicle, and subsequent rotation of the vehicle in pitch and roll produces translation. Alternately, translation can be achieved through cyclic motion of vertical surfaces mounted at the tips of the rotating wings (winglets) which produce translational forces directly. Note that cyclic pitch will still be required to provide moment balance in forward flight.

Alternate shapes for the buoyant centerbody in conjunction with winglet control have been considered to improve the translational performance of the concept. In the experimental investigation to be described, only cyclic pitch was used for control; however, the effectiveness of winglets as a control

Received July 24, 1979; revision received Feb. 11, 1980.

Index categories: Handling Qualities, Stability and Control; Helicopters; Lighter-than-Airships.

*Prof., Dept. of Mechanical and Aerospace Engineering. Member AIAA.

†Senior Technical Staff Member, Dept. of Mechanical and Aerospace Engineering.

Table 1 Aerocrane dynamic model characteristics

Rotor diameter	12.2 m	Empty weight	80 kg
Centerbody diameter	5.5 m	Payload	46 kg
Rotational velocity	30 rpm	Buoyant lift	965 N

Dimensionless parameters of Aerocrane

	Dynamic model	Proposed design
Wing tip acceleration, g	6	5.6
Buoyancy-empty weight ratio	1.15	1.4
Payload-empty weight ratio	0.6	0.85
Thrust-payload ratio	0.75	0.5
Thrust coefficient-solidity ratio	0.045	0.033

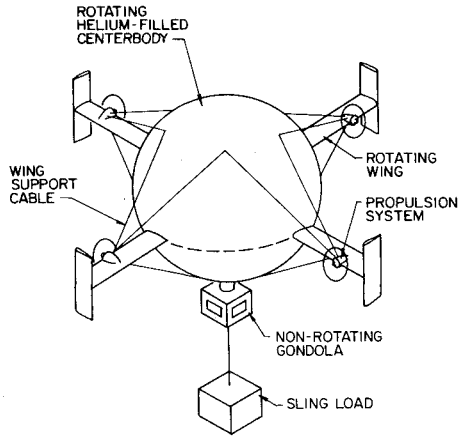

Fig. 1 Aerocrane configuration.

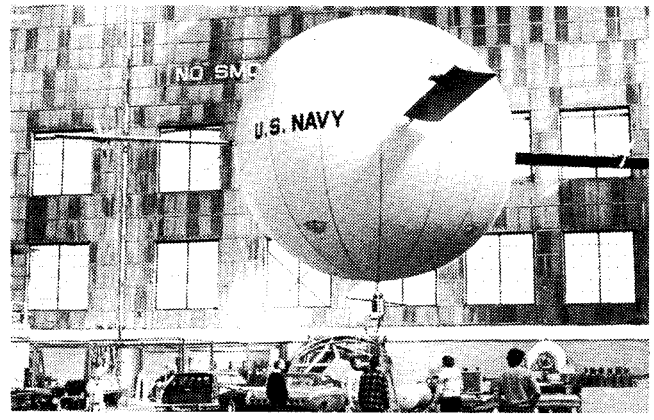

Fig. 2 Dynamic model of Aerocrane.

method was studied theoretically. The basic configuration is appealing owing to its relative simplicity.

Essential to the evaluation of the potential of this hybrid concept is the development of a quantitative understanding of its dynamic stability and maneuverability characteristics especially near hover. Owing to the unusual vehicle configuration, as well as the emphasis on flight behavior and maneuverability at very low flight speeds, it was decided that the most suitable approach was to conduct an experimental investigation using a relatively large (overall diameter 12.2 m) Froude-scaled dynamic model in free flight, rather than the more conventional approach of wind-tunnel testing. The large size of the model was selected for two reasons: 1) to obtain a sufficiently high Reynolds number such that the aerodynamic forces acting on the centerbody could be considered representative of full-scale flight; and 2) in the design of a Froude-scaled model incorporating buoyant lift, scaling of various physical components dictates a relatively large size. Pertinent dimensions of the model are given in Table 1, along with important dimensionless parameters of the model as well as those of a proposed full-scale design. The model was fully instrumented such that its flight behavior could be quantitatively measured.

From the dimensionless parameters given in Table 1 certain design features can be noted. The tip speed of the rotating wings is low and the acceleration at the tips of the rotating wings is approximately 6 *g*'s, considerably smaller than a helicopter. The thrust coefficient-solidity ratio is approximately 0.04, also smaller than a conventional helicopter, i.e., the rotating wings are lightly loaded even at full payload. The buoyant force to empty weight ratio for a proposed full-scale vehicle is 1.4 so that the vehicle has excess buoyancy without payload. This ratio is smaller on the model owing to a higher specific weight of various components compared to a full-scale vehicle. The design payload to empty weight ratio is 0.84 giving a thrust-to-payload weight of 0.5, i.e., when fully loaded the rotating wings are lifting one-half of the payload. Without payload, vertical equilibrium is achieved by thrusting downward. Only the flight characteristics with full payload were examined in this study.

All experiments with the model were conducted in a gust-free environment within a large airship hangar at Lakehurst, New Jersey.

This paper describes the results of the experimental investigation conducted with the free-flight model and compares these data with theory. Very good agreement was obtained between theory and experiment. This experimentally verified theoretical model was employed in a real-time simulation to evaluate the precision hover capabilities of the concept. The results are compared with similar studies of heavy-lift helicopters and the specifications for helicopter handling qualities. Predicted full-scale characteristics are presented for 16- and 50-ton payload Aerocranes.

Experimental Investigation

Figure 2 shows the Froude-scaled dynamic model of the Aerocrane equipped with a sling load. This model may be considered a one-tenth scale dynamic model of a 50-ton payload Aerocrane. This model was powered by electric motors and controlled by an operator in a chase vehicle which kept station on the model as it was flown along the length of the building. Model control was provided by a fly-by-wire system consisting of servomechanisms at the root of each blade, which received suitable inputs from an electronic swashplate in the nonrotating gondola. Although the model was stable in hovering flight, it was found desirable to provide a relatively simple attitude feedback system. The stabilization system was found quite useful during the initial flights when the operator was learning to fly the model, as pitch and roll cues were difficult to obtain since the model was flown quite high above the building floor to minimize ground effects. After gaining experience with the model, the operator found that while the attitude feedback was helpful, it was not necessary for making controlled flights.

Experimental investigations included steady trimmed flights along the length of the enclosure at translational speeds up to 3.8 m/s (12 m/s equivalent on a 50-ton payload vehicle). During the flights, continuous measurement of vehicle pitch and roll attitudes, airspeeds, and collective and cyclic control positions were made. At maximum translational speed (3.8 m/s), a nose-down pitch attitude of 30 deg and a left roll of 17 deg was required for equilibrium.

After these experiments were completed, in order to evaluate the dynamic stability and control characteristics, cyclic pulse inputs were applied at a number of steady flight conditions, and the time histories of vehicle motion in response to this input were recorded. Figure 3 shows typical responses at various flight conditions. Note that unlike the conventional helicopter, the vehicle transient motion, although lightly damped, is stable near hovering and becomes more stable as translational velocity increases. The theoretical model described below indicated that the stability is not very sensitive to either sling-load geometry or vertical center of gravity location. The center of gravity of the vehicle is located below the center of buoyancy and contributes to the stability.

Further examination of the transient motion in hover shows a pitch and roll symmetry which arises because the pitch and roll inertias are equal. This symmetry implies that the dynamic response of the vehicle to a cyclic control input is in fact a circling or whirling motion. The circular nature of the transient response characteristic was, to a large extent, responsible for the initial difficulties experienced by the ground operator in controlling the vehicle. The period of this lightly damped mode in hovering is relatively long (12 s for the model, 36 s scaled to the 50-ton vehicle) and would not be expected to produce any piloting problems for an operator in the vehicle who would have the advantage of vehicle motion cues. The levels of pitch/roll coupling are similar to those of a single rotor helicopter.

The theory developed to predict these experimental results is described in the next section.

Theory

A theoretical model describing the hovering dynamics and control characteristics of the Aerocrane was developed. The sling load is not included here. The equations of motion, including the effects of the sling load, are given in Ref. 1. A small perturbation model was employed for the hovering flight analysis. Linear equations of motion result with the exception of the forces associated with centerbody drag and Magnus effect. Owing to the large values of the drag and Magnus force coefficients determined from the equilibrium flight experiments, these nonlinear effects were retained in the stability analysis.

The assumption of small perturbations about equilibrium hovering flight uncouples the vertical translation and yaw from the other degrees of freedom. Thus a four-degree-of-freedom model is used to investigate the hovering dynamics and control without the sling load. A body-axis system with the z axis aligned with the axis of rotation is employed. The x axis points forward and the y axis points to the right. The four equations of motion consisting of the summation of the pitch and roll moments about the center of gravity and the summation of longitudinal and lateral forces can be written as

$$I_0\dot{p}+I_z\Omega q=L_B, \qquad I_0\dot{q}-I_z\Omega p=M_B \tag{1}$$

$$m_0\dot{u}=X_B, \qquad m_0\dot{v}=Y_B$$

Note that the rotor rotates in a clockwise direction when viewed from the top. The external forces and moments arise from the following sources: buoyant forces acting on the helium-filled centerbody, aerodynamic forces acting on the centerbody proportional to acceleration ("apparent mass"), centerbody drag and Magnus forces, aerodynamic forces and moments acting on the rotating blades, and gravity forces. In steady hovering flight, the vertical equilibrium equation is

$$W-F_B-T_S=0 \tag{2}$$

It is assumed that there is no aerodynamic interaction between the rotor and the centerbody. Various qualitative experiments were conducted with an isolated rotating sphere which indicated that when a sphere is rotated, the size of the turbulent wake is reduced and, in addition, that the fluctuations in the forces become very small. No unusual vibrations or other aerodynamic effects were observed during the flights of the model which could be associated with aerodynamic interactions between the centerbody and the rotating wings. While these interference effects may be important in the performance analysis, e.g., the rotor in-flow may produce a download on the spherical centerbody and the

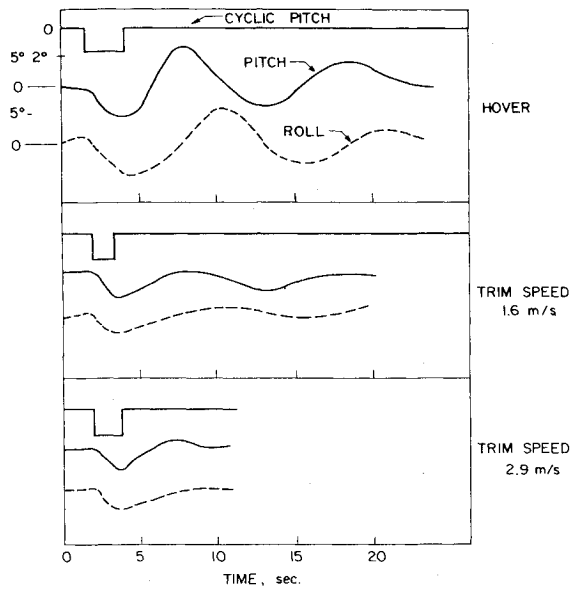

Fig. 3 Measured transient response characteristics of Aerocrane dynamic model at various trim speeds.

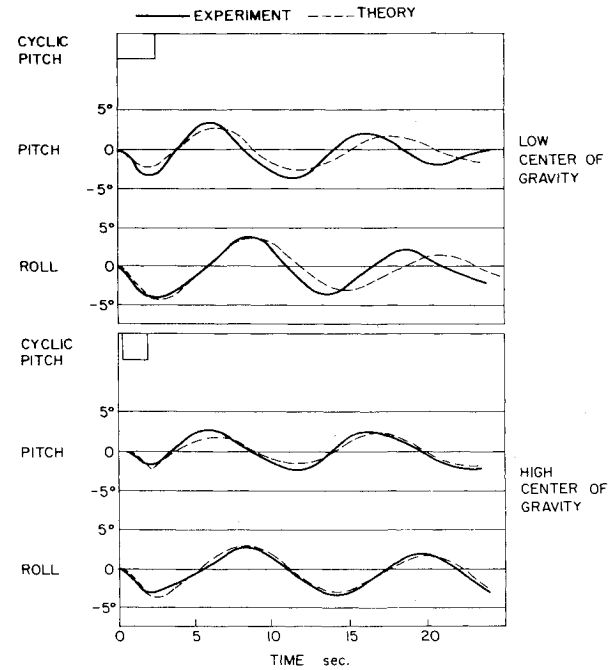

Fig. 4 Transient response characteristics of Aerocrane dynamic model, comparison of theory and experiment in hovering flight.

presence of the centerbody may influence the rotor in-flow distribution, affecting the rotor blade twist distribution for optimum rotor performance, it was assumed that these effects would not be significant in the stability and control analysis.

Buoyancy and gravity produce the following contributions to the body forces for small pitch and roll angles

$$\Delta X_{BB} = -(W-F_B)\theta, \qquad \Delta Y_{BB} = (W-F_B)\phi \tag{3}$$

The buoyant force also produces restoring moments, since the center of gravity is located a distance r_0 below the center of buoyancy

$$\Delta L_{BB} = -F_B r_0 \phi, \qquad \Delta M_{BB} = -F_B r_0 \theta \tag{4}$$

Aerodynamic forces are produced by an accelerating sphere. Potential flow theory yields the result that these forces act at the center of buoyancy of the sphere and are equal to one-half the volume of the sphere times the fluid density times the acceleration at the center of buoyancy. Since the center of gravity of the vehicle is located below the center of buoyancy, moments as well as forces are produced. The acceleration of the center of buoyancy in terms of the center of gravity motion is

$$a_{x_{CB}} = \dot{u} - r_0 \dot{q}, \qquad a_{y_{CB}} = \dot{v} + r_0 \dot{p} \tag{5}$$

and, therefore, the contributions of the aerodynamic acceleration forces to the equation of motion are

$$\Delta X_{BA} = -m_A(\dot{u} - r_0\dot{q}), \qquad \Delta Y_{BA} = -m_A(\dot{v} + r_0\dot{p})$$

$$\Delta L_{BA} = -r_0 m_A(\dot{v} + r_0\dot{p}) \qquad \Delta M_{BA} = -r_0 m_A(\dot{u} - r_0\dot{q}) \tag{6}$$

where

$$m_A = \tfrac{1}{2}\rho V \tag{7}$$

The centerbody drag and Magnus contributions can be expressed as

$$\Delta X_{BD} = -\tfrac{1}{2}\rho S C_D u|u| - \tfrac{1}{2}\rho S C_{L_M} v|v| \tag{8}$$

$$\Delta Y_{BD} = -\tfrac{1}{2}\rho S C_D v|v| + \tfrac{1}{2}\rho S C_{L_M} u|u|$$

Moments are also produced about the center of gravity

$$\Delta L_{BD} = r_0 \Delta Y_{BD}, \qquad \Delta M_{BD} = -r_0 \Delta X_{BD} \tag{9}$$

The rotor blades give rise to hub moments and in-plane forces. The rotating blades were assumed to be rigid in the flapping or out-of-plane direction as a consequence of the low angular velocity of the rotor, coupled with the external bracing of the rotor blades, which yields a first-mode out-of-plane blade bending frequency well above one per revolution.

Blade element theory is employed to predict the forces and moments produced by the rotor. Simple momentum theory is used to determine the relationship between thrust and induced velocity. Since the rotor is assumed to be rigid and, therefore, can produce aerodynamic moments, it is necessary to extend the momentum theory to include first-harmonic components of the induced velocity.[4] In addition, an harmonic component of the induced velocity arising from the blowback of the rotor wake is included.[5]

$$\frac{v}{\Omega R} = -\lambda_0 - (\lambda_B + \lambda_M)\cos\psi_w - \lambda_L \sin\psi_w \tag{10}$$

where for a rigid-wake model, momentum theory gives the constant component of the induced velocity in hovering flight as

$$\lambda_0 = -\sqrt{C_T/2f_2} \tag{11}$$

where f_2 is a factor accounting for the fact that the rotor blade radius extends only to the spherical centerbody. Denote in the following,

$$f_n = 1 - (R_B/R)^n \tag{12}$$

λ_B is the harmonic component of the induced velocity arising from the blowback of the wake, and is assumed to vary linearly along the fore and aft diameter of the disk following Ref. 5. Therefore.

$$\lambda_B = \lambda_1 x \tag{13}$$

The results of Ref. 5 can be approximated near hover to yield

$$\lambda_1 \cong -(\mu_s/2) \tag{14}$$

However, comparison of theory and experiment in this study, as well as the results of Ref. 6, indicate that this theoretical result is about a factor of two too small. Therefore, the value used in this study was taken to be twice that given by Eq. (14)

$$\lambda_1 \cong -\mu_s \tag{15}$$

This factor of two tends to account for the fact that the hub moment produced by a rigid rotor is very sensitive to the radial distribution of this harmonic component of the induced velocity and the linear distribution is apparently in error near the tips of the blades.

The harmonic components λ_M and λ_L are assumed to be proportional to the aerodynamic moments produced by the rotor, i.e.,

$$\lambda_M = j(2C_M/a\sigma); \qquad \lambda_L = -j(2C_L/a\sigma) \tag{16}$$

The factor j is determined from momentum theory.

An angular momentum balance on the rotor yields the value of j as

$$j = \eta \frac{a\sigma}{|\lambda_s|} \tag{17}$$

where η is a numerical constant whose magnitude depends upon two assumptions: rigid or nonrigid wake, and the radial distribution of induced velocity. A value of η equal to one-half was used based on the experimental data presented in Ref. 7. One-half is approximately the average of the value of η obtained from the rigid and nonrigid wake model assuming that the harmonic components are independent of radius.

With this model for the induced velocity, expressions for the rotor forces and moments can be developed. In a body-

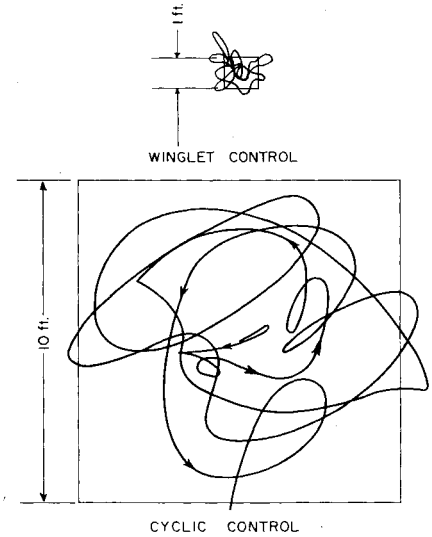

Fig. 5 Simulation results for ground track of 16T Aerocrane, hovering over a spot in 1.5 m/s random gusts.

wind axis system, the following results are obtained from blade element theory coupled with the model for the induced velocity described above. Terms involving the square of the advance ratio have been dropped since near-hovering flight is of interest.

$$\frac{2C_{M_{s,w}}}{a\sigma} = \frac{1}{1+\frac{a\sigma}{12|\lambda_s|}f_3}\left[\frac{A_{1_{s,w}}}{8}f_4 - \frac{1}{8}\left(\frac{q_{s,w}}{\Omega}+\lambda_1\right)f_4\right] \tag{18}$$

$$\frac{2C_{L_{s,w}}}{a\sigma} = \frac{1}{1+\frac{a\sigma}{12|\lambda_s|}f_3}\left[-\frac{B_{1_{s,w}}}{8}f_4 - \frac{1}{8}\frac{p_{s,w}}{\Omega}f_4 + \mu_s\left(\frac{\theta_0}{3}f_3+\frac{\lambda_s}{4}f_2\right)\right] \tag{19}$$

λ_M and λ_L have been eliminated using Eqs. (16) and (17). The rotor in-plane forces are:

$$\frac{2C_{H_{s,w}}}{a\sigma} = \frac{\delta\mu_s}{2\alpha}f_2 - \frac{1}{2}\theta_0\left(\lambda_L\frac{f_2}{2} - \frac{p_{s,w}}{\Omega}\frac{f_3}{3} + \mu_s\lambda_s f_1\right) + B_{1_{s,w}}\left[\lambda_s\frac{f_2}{4} + \frac{3}{8}\mu_s\left(\lambda_L f_1 - \frac{p_{s,w}}{\Omega}\frac{f_2}{2}\right)\right] + \frac{\mu_s A_{1_{s,w}}}{8}\left(\lambda_M f_1 + \frac{q_{s,w}}{\Omega}\frac{f_2}{2} + \lambda_1\frac{f_2}{2}\right) - \lambda_s\left(\lambda_L f_1 - \frac{p_{s,w}}{\Omega}\frac{f_2}{2}\right) \tag{20a}$$

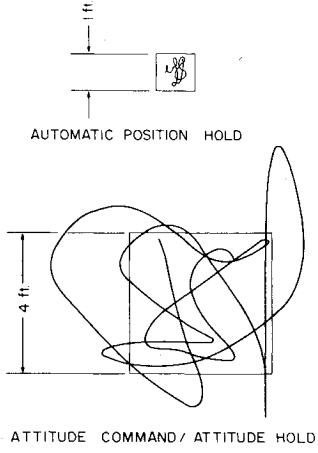

Fig. 6 Simulation results for heavy lift helicopter,[8] hovering over a spot in 1.5 m/s random gusts.

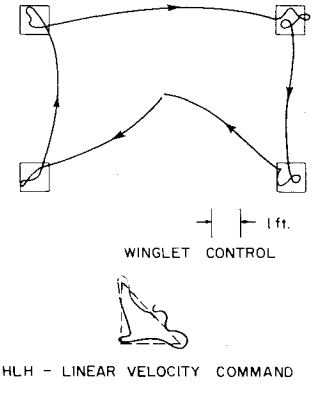

Fig. 7 Simulation results for point-to-point translation, Aerocrane and heavy lift helicopter, no gusts.

$$\frac{2C_{Y_{s,w}}}{a\sigma} = -\frac{\theta_0}{2}\left(\lambda_1\frac{f_3}{3} + \lambda_M\frac{f_2}{2} + \frac{q_{s,w}}{\Omega}\frac{f_3}{3}\right) + A_{1_{s,w}}\left(\lambda_s\frac{f_4}{4} + \frac{\mu_s}{8}\lambda_L f_1 - \frac{p_{s,w}}{\Omega}\frac{f_2}{16}\right) + \frac{B_{1_{s,w}}\mu_s}{8}\left(\lambda_M f_1 + \frac{q_{s,w}}{\Omega}\frac{f_2}{2} + \lambda_1\frac{f_2}{2}\right) - \lambda_s\left(\lambda_M f_1 + \lambda_1\frac{f_2}{2} + \frac{q_{s,w}}{\Omega}\frac{f_2}{2}\right) \tag{20b}$$

The rotor operating conditions are determined from the thrust coefficient expression. For steady flight,

$$(2C_{T_{s,w}}/a\sigma) = \theta_0(f_3/3) + (\lambda_s - \mu_s B_{1_{s,w}})(f_2/2) \tag{21}$$

The in-flow ratio and the advance ratio near hovering flight can be expressed as

$$\lambda_s = \lambda_0 \tag{22}$$

and

$$\mu_s = (\bar{u}^2 + \bar{v}^2)^{1/2} \tag{23}$$

The following transformation converts the rotor forces, moments, cyclic, and vehicle angular rates from the wind orientation to the body orientation,

$$\begin{Bmatrix} X_{BR} \\ Y_{BR} \end{Bmatrix} = \frac{1}{(\bar{u}^2+\bar{v}^2)^{1/2}}\begin{bmatrix} \bar{u} & \bar{v} \\ -\bar{v} & \bar{u} \end{bmatrix}\begin{Bmatrix} X_{B,W} \\ Y_{B,W} \end{Bmatrix} \tag{24}$$

where

$$\begin{Bmatrix} X_{B,W} \\ Y_{B,W} \end{Bmatrix} = \begin{Bmatrix} -C_{H_{s,w}} \\ C_{Y_{s,w}} \end{Bmatrix}, \begin{Bmatrix} C_{L_{s,w}} \\ C_{M_{s,w}} \end{Bmatrix}, \begin{Bmatrix} A_{1_{s,w}} \\ B_{1_{s,w}} \end{Bmatrix}, \begin{Bmatrix} p_{s,w} \\ q_{s,w} \end{Bmatrix}$$

where X_{BR} and Y_{BR} represent corresponding quantities in the body-axis system.

Since the rotor forces act in the plane of the rotor, the moment contributions of the rotor about the center of gravity are:

$$\Delta L_{BR} = \Delta L_{RH} + r_0\Delta Y_{BR} \qquad \Delta M_{BR} = \Delta M_{RH} - r_0\Delta X_{BR} \tag{25}$$

where the rotor hub moments are given in dimensionless form in Eq. (20). The external forces and moments in Eq. (1) are obtained by summing contributions given by Eqs. (3,4,6,8,9,24, and 25), along with the rotor forces and moments given in Eqs. (18-20).

Thus this completes the development of the equation of motion employed to predict the dynamic stability characteristics and control response of the vehicle.

The transient response characteristics shown also include the effect of sling load described by two additional degrees of freedom, as well as a small contribution from the umbilical cable carrying power to the model.

A theoretical model for the contribution of the winglets is presented in Ref. 3. Winglets were employed in the simulation study described, but not in the dynamic model tests.

Comparison of Theory and Experiment

The theory described in the previous section was employed to predict the transient response to control in hovering flight for comparison with experiment. Figure 4 shows the comparison between the measured and predicted pulse response in hover indicating very good agreement. As mentioned previously, the theory incorporated drag and Magnus force coefficients which were determined from the steady flight experiments. The theoretical expressions for the rotor in-plane forces indicated that, in general, in all flight conditions they could be neglected in comparison to the centerbody

forces. Measured model pitch and roll attitudes, therefore, could be used to determine the drag and Magnus force coefficients. Trim attitudes with a variety of payloads and center-of-gravity positions were predicted very well with $C_D = 0.80$ and $C_{L_M} = 0.30$. These nonlinear terms were not significant in the stability and control analysis, except in the case where the control inputs were much larger than those employed in the model flight test program. Also, the value of the first harmonic component of the induced velocity arising from the blowback of the wake was taken to be twice the theoretical value of Ref. 5. The pitching moment variation with translational velocity arises primarily from this effect and is the stability derivative that essentially determines the damping of the hovering transient motion.

These comparisons indicated that a sound theory to predict the flight behavior of the Aerocrane has been developed. Consequently, the equations of motion were scaled to a 16-ton payload configuration and used to study the precision hover capabilities of the concept.

Precision Hover Capabilities

Since a linearized theoretical model for vehicle response showed good agreement with experimental data, the simplest approach to a real-time simulation was to employ an analog computer. The vehicle plus sling load was modeled as a six-degree-of-freedom system as discussed. Height control was not examined. Random gust disturbances were included in the simulation study. Cyclic pitch and winglet control were examined and compared. The winglets were modeled theoretically, as no experiments were conducted with winglets. Winglet area was selected to be of sufficient size to trim the model in level flight with zero pitch attitude at the maximum translational speed (model scale) 3.8 m/s. A winglet span to rotor radius of 0.25 was required. This size winglet produces approximately 0.023 *gs* per degree of winglet cyclic deflection in hover.

For the simulation study, the operator or pilot was given two tasks to accomplish. First hovering over a designated spot was attempted with 1.5 m/s rms gust disturbances. For the second task, the operator attempted to fly from one position to an adjacent position, stop, and then continue to another spot. No gusts were employed in this task. It should be noted that a very simple simulator configuration was used. No cockpit was used and no attitude information was provided for the operator. The vehicle was flown by observing its track in the horizontal plane on an *X-Y* plotter. This admittedly makes the selected tasks difficult. However, it was considered that this simple experimental configuration would provide a valid basis for examining the relative merits of cyclic and winglet control, as well as giving indications of the comparison of control characteristics of the Aerocrane with large helicopters.

First, consider the task of hovering over a spot in the presence of gusts. Results showing ground track of the Aerocrane over a few minutes of simulated flight are shown in Fig. 5. To accomplish this task with cyclic control, attitude feedback was found necessary. The operator was able to stay within a 10 ft square for a relatively long period of time. A dramatic improvement in the ability to hover over a spot is shown with winglet control as would be expected from various helicopter handling qualities studies. Corresponding results taken from a simulation study of a heavy-lift helicopter are shown in Fig. 6.[8] Conventional control of the helicopter with an attitude hold system indicates somewhat better performance than the Aerocrane with cyclic control. It was possible to maintain the helicopter within a 4 ft square. For the heavy-lift helicopter equipped with a sophisticated control system involving automatic position hold, the displacements are only slightly better than the unstabilized Aerocrane with winglet control.

With cyclic control, translation from point to point was found to be very difficult for the Aerocrane. This difficulty appears to be related to a general problem associated with semibuoyant vehicles carrying heavy sling loads and employing moment controls as discussed later.

A typical simulation run of the Aerocrane employing winglet control is shown in Fig. 7. A smooth transition from point to point was achieved and the results are quite similar to the heavy-lift helicopter results with a translational velocity command system which is also shown in the figure. Again, recall that the Aerocrane had no automatic stabilization system.

Upon detailed examination, the difficulty of translating from point to point with the Aerocrane using cyclic control appears, to a large extent, to be a result of the effect of sling load motion on vehicle translational motion. The effect of the sling load inertia is considerably more pronounced as a result of the fact that the vehicle is supported in part by buoyant forces; thus the aerodynamic thrust force, which produces translation, is small.

The following simplified model indicates that this behavior appears to be characteristic of any hybrid system in which translation is produced by rotation of the vehicle near hover. If we assume that the pilot's control commands vehicle attitude, then the angular dynamics of the vehicle are eliminated from the equations of motion and the interaction of the sling load and the vehicle can be treated as a forced-response problem[3] (i.e., for motion in any direction, the vehicle is modeled as a two-degree-of-freedom system). Vehicle attitude

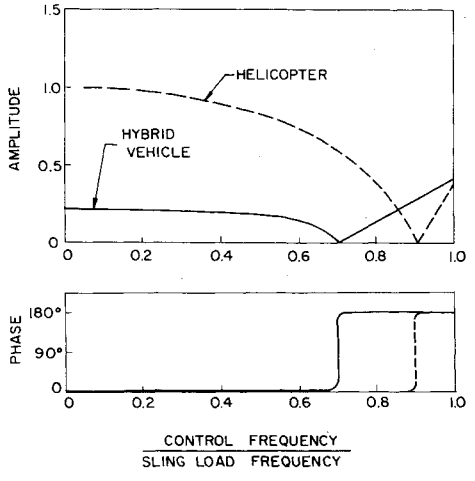

Fig. 8 Translational acceleration to pitch attitude frequency response, comparison of hybrid vehicle and helicopter.

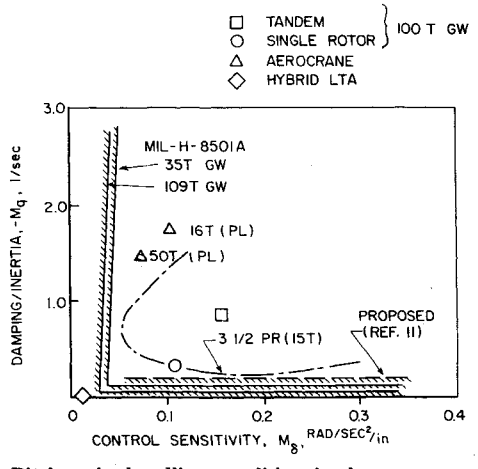

Fig. 9 Pitch axis handling qualities in hover, comparison of Aerocrane and large helicopters with Refs. 9 and 10, and Hybrid LTA of Ref. 12.

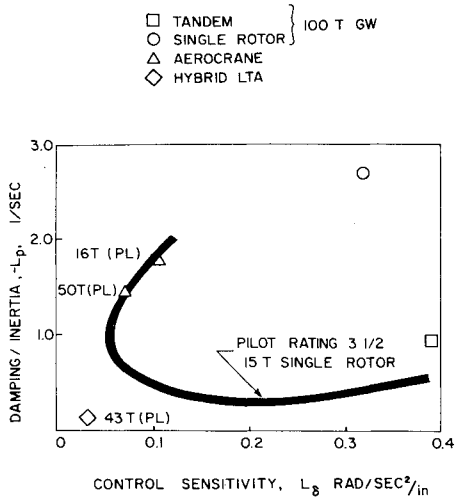

Fig. 10 Roll axis handling qualities in hover.

is taken to be the system input, and translational acceleration and sling load motion are outputs. With this simplification, the equations of motion become independent of the details of the vehicle configuration. The only parameters that enter the equations are the sling load geometry and the relative magnitudes of the aerodynamic thrust, buoyant force, payload, and vehicle empty weight.

Figure 8 shows the frequency response of horizontal acceleration to pitch attitude for the Aerocrane as a function of the ratio of pilot input frequency to sling load pendulous frequency. Typical helicopter characteristics are also shown for comparison purposes. Owing to the presence of the buoyant force and, consequently, the low thrust of the Aerocrane, low-frequency inputs produce small translational accelerations due to attitude compared to the helicopter. If the pilot attempts to obtain a more rapid response by increasing the frequency of control, first the acceleration amplitude decreases, and then, at an input frequency above about 70% of the sling load frequency, the phase of the acceleration response shifts 180 deg, indicating that translational acceleration is now occurring in a direction opposite to the tilt. The sling load dynamic motions are, in fact, driving the vehicle. This unusual behavior was very evident in the simulation with the complete dynamic model when attempting to translate from point to point with cyclic control. It seems worthwhile to re-emphasize that this behavior is likely to be characteristic of any hovering vehicle carrying a large sling load, which obtains an appreciable fraction of its lift from buoyancy and is translated by tilting.

As a final note, it is interesting to examine the Aerocrane characteristics with cyclic control in light of the U.S. Military Helicopter Flying Qualities Specifications.[9] Shown in Fig. 9 on the control sensitivity-damping plane are the estimated pitch-axis characteristics of a 16- and 50-ton payload Aerocrane compared with suitably scaled single and tandem rotor helicopters. The Aerocrane configuration is characterized by relatively high levels of angular damping compared to the helicopters and low levels of control sensitivity (control gearing 3 deg cyclic/in.). The Aerocrane does fall within the satisfactory boundaries given by Ref. 9; it should be realized, however, that a significant extrapolation of criteria is involved as the gross weight trends given in Ref. 9 have only been verified for helicopters up to 15 tons gross weight.[10] A pilot opinion boundary of three and one-half, representing a marginally satisfactory rating on the Cooper-Harper scale determined in Ref. 10, is also shown in Fig. 9. The Aerocrane control characteristics in hover appear to be similar to those expected for large helicopters.

Other opinions can be found in the literature relating to the manner in which these criteria depend upon size when very large vehicles are examined. A minimum damping level, also shown in Fig. 9, is proposed in Ref. 11. It is clear that a detailed review of the applicability of these criteria to very large vehicles is needed.

Also shown in Fig. 9 are the values of the control sensitivity and damping for another hybrid LTA vehicle consisting of four helicopter rotors attached to an airship hull.[12] The control sensitivity is calculated for a total stick travel of 4 in. using the control power from Ref. 12. The angular damping was obtained from Ref. 13. This concept shows extremely low levels of control power and damping compared to the Aerocrane, as well as not meeting the helicopter specifications. These results indicate that it may be very difficult to achieve precision hover capabilities with this concept.

Figure 10 shows similar comparisons for the roll axis where, in this case, the Aerocrane characteristics fall on the three and one-half pilot rating boundary determined for a 15-ton helicopter. Again, the results of Ref. 12 indicate very low levels of control sensitivity for the hybrid configuration.

Concluding Remarks

The Aerocrane configuration results in a vehicle that is readily controllable and maneuverable in hovering and low-speed flight with full payload. Its hovering control characteristics appear to be similar to what would be expected of large helicopters. Very effective maneuvering control around hover can be achieved through the use of winglets. With a spherical centerbody and cyclic pitch, comparatively large attitudes are required for trimmed flight at moderate speeds.

An experimentally verified theoretical model has been developed which should prove valuable for additional design studies of this concept.

Acknowledgment

This research was supported by the Naval Air Development Center, Warminster, Pa. under Contracts N62269-76-C-0464 and N62269-77-C-0074.

References

[1] Putman, W.F. and Curtiss, H.C., Jr., "An Analytical and Experimental Investigation of the Hovering Dynamics of the AEROCRANE Hybrid Heavy Lift Vehicle," Princeton University, AMS TR 1291, June 1976.

[2] Putman, W.F. and Curtiss, H.C., Jr., "An Experimental and Analytical Investigation of the Hovering and Forward Flight Characteristics of the AEROCRANE Hybrid Heavy Lift Vehicle," Naval Air Development Center Rept. NADC-76201-30, Sept. 1977.

[3] Curtiss, H.C., Jr., Putman, W.F., and McKillip, R.M., Jr., "A Study of the Precision Hover Capabilities of the AEROCRANE Hybrid Heavy Lift Vehicle," Naval Air Development Center Rept. NADC-76341-30, Feb. 1978.

[4] Curtiss, H.C., Jr., "Complex Coordinates in Near Hovering Rotor Dynamics," *Journal of Aircraft*, Vol. 10, May 1973, pp. 289-296.

[5] Coleman, R.P., Feingold, A.M., and Stempin, C.W., "Evaluation of the Induced Velocity Field of an Idealized Helicopter Rotor," NACA Wartime Rept. ARR L5E10, June 1945.

[6] Harris, F.D., "Articulated Rotor Blade Flapping Motion at Low Advance Ratio," *Journal of the American Helicopter Society*, Vol. 17, Jan. 1972., pp. 41-48.

[7] "Static Tests on A Full-Scale Boeing-Vertol 76 Rigid Propeller," *Boeing Company, Vertol Division: Experimental Programs Conducted Under the U.S. Army Cart Loan Agreement*, Vol. I, Boeing-Vertol Rept. R-339, June 1965.

[8]Davis, J.M., Landis, K.H., and Leet, J.R., "Development of Heavy Lift Helicopter Handling Qualities for Precision Hover," American Helicopter Society Preprint 940, May 1975.

[9]Anon, "Military Specifications Helicopter Flying and Ground Handling Qualities: General Requirements for," MIL-H-8501A, Sept. 1961.

[10]Tapscott, R.J. and Sommer, R.W., "A Flight Study with a Large Helicopter Showing Trends of Lateral and Longitudinal Control Response with Size," NASA TND-3600, Sept. 1966.

[11]Szustak, L.S. and Jenney, D.S., "Control of Large Crane Helicopters," American Helicopter Society Preprint 441, June 1970.

[12]Meyers, D.N., "Hybrid LTA Vehicle Controllability as Affected by Thruster Magnitude and Spacing," Naval Air Development Center Rept. NADC 76327-30, July 1977.

[13]Nagabhushan, B.L. and Tomlinson, N.P., "Flight Dynamics Analyses and Simulation of Heavy Lift Airships," AIAA Paper 79-1593, AIAA Lighter-than-Air Systems Technology Conference, July 11-13, 1979, Palo Alto, Ca.